Mode conversion and scattering of Lamb waves at delaminations in composite laminates

Gnana Teja Pudipeddi

Graduate Student, School of Civil, Environmental and Mining Engineering,

The University of Adelaide, Adelaide, South Australia, 5005, Australia.

Email: gnanateja.pudipeddi@adelaide.edu.au

Ching-Tai Ng

Associate Professor, School of Civil, Environmental and Mining Engineering,

The University of Adelaide, Adelaide, South Australia, 5005, Australia (Corresponding author).

Email: alex.ng@adelaide.edu.au

Andrei Kotousov

Professor, School of Mechanical Engineering, The University of Adelaide, Adelaide, South Australia, 5005, Australia.

Email: andrei.kotousov@adelaide.edu.au

Abstract:

This paper presents a study of Lamb wave scattering and mode conversion at a delamination in quasi-isotropic (QI) composite laminates. The study employs the fundamental anti-symmetric mode (A_0) Lamb wave as the incident wave, and investigates the A_0 scattered Lamb wave and mode converted fundamental symmetric mode (S_0) Lamb wave (A_0-S_0) at the delamination. A three-dimensional (3D) explicit finite element (FE) model is proposed to

predict the Lamb wave propagation in the QI composite laminates, and A_0 scattered wave and A_0-S_0 mode converted wave at the delamination. An experimental study is also carried out to demonstrate that the 3D FE model is able to provide a reasonable prediction of the A_0 and S_0 Lamb wave propagation in the QI composite laminates. The results show that the amplitudes of the A_0 scattered and A_0-S_0 mode converted Lamb wave depend on the fibre orientation of the outer laminae, and the size and through-thickness location of the delamination. In summary the results of this study can further advance the delamination detection techniques using Lamb wave and gain physical insights into the scattering and mode conversion of Lamb wave at the delamination.

Keywords: Lamb wave, scattering, mode conversion, finite element, composite laminate, delamination

Introduction

Fibre-reinforced composite laminates have been widely employed in different engineering fields, such as aerospace, civil and automobile industries, due to their light weight, corrosion resistance and high stiffness properties (Hollaway 2010). The composite laminates are fabricated by assembling layers of fibrous composite materials. The flexural strength of the composite laminates highly depends on shear transfer between each lamina, and hence, the separation of adjacent laminae could significantly reduce its flexural strength. This kind of separation or slippage between the laminae is called delamination. Delaminations are invisible on the surface of the composite laminates, and hence, it is hard to be effectively and reliably detected (Liu *et al*. 2019).

The detection of delamination requires reliable non-destructive evaluation (NDE) techniques (Ibrahim 2014). In the last two decades, different NDE techniques were developed

to detect the delamination in the composite laminates, for example, conventional ultrasonic (Kazys & Svilainis 1997; Imielinska *et al*. 2004), thermography (Avdelidis *et al*. 2003; Sinha *et al*. 2015), eddy current (Mook *et al*. 2001; Mizukami *et al*. 2015), vibration based techniques (Zhang *et al*. 2016; Zhang *et al*. 2017; Pan *et al*. 2018), guided wave techniques (Ng 2015a; He & Ng 2017) and nonlinear ultrasonic techniques (Soleimanpour & Ng 2017; Yang *et al*. 2018). In particular, guided wave techniques have been widely recognised as one of the cost-effective and reliable approaches.

Developments of damage detection using Lamb waves

Lamb waves are guided wave propagation in thin plates, such as composite laminates. It has been widely demonstrated that Lamb waves are sensitive to subsurface damage and can be used to inspect large area (Kessler *et al*. 2002; Diamanti *et al*. 2004). The development of using Lamb waves in damage detection can be categorised into two groups, development of damage detection technique using Lamb waves and fundamental understanding of Lamb waves interaction with the damage.

In the last decade, different studies were carried out to investigate the scattering characteristics of Lamb wave in different types of damages. The phenomena of Lamb wave scattering at different types of damage, such as through hole (Diligent *et al*. 2002; Fromme & Sayir 2002), blind hole (Grahn 2003; Cegla *et al*. 2008), crack (Flores-Lopez & Gregory 2006; Ratassepp *et al*. 2008), and corrosion (Moreau *et al*. 2012) in isotropic plates were studied in detail.

At the same time, different damage detection techniques using Lamb wave were developed to detect damages in structures (Ng 2015b; Sherafat *et al*. 2018; Yang *et al*. 2018). These methods rely on linear features of Lamb waves scattered from defects to achieve damage detection and identification. He and Ng (2016) proposed a model based approach

using Lamb waves reflected from delaminations to provide a quantitative damage identification in laminated beams. Singh *et al*. (2017) proposed to use the reflected and transmitted Lamb waves at the delamination to provide damage identification in composite laminates. Pieczonka *et al*. (2017) employed the information of the mode-converted Lamb waves to detect the damage in composite panels. Lu *et al*. (2017) proposed a delay-and-sum imaging algorithm to identify bonded mass damage using Lamb waves. Aryan *et al*. (2017) proposed to use 3D laser vibrometry to measure mode converted Lamb waves from the damage to reconstruction an image for damage identification.

Most of the damage detection methods using linear features of Lamb waves require reference signals to extract the scattered waves from the damage. But Lamb waves are sensitive to the change of environmental conditions, such as varying temperature or loading conditions, and this can make baseline subtraction fail to extract the scattered wave signals form the measured data. To further enhance the practicability of using Lamb waves for damage detection, different approaches have been proposed to minimise the environmental effect in the baseline subtraction. Croxford *et al*. (2010) proposed an optimal baseline selection and baseline signal stretch approach to compensate the temperature effect of Lamb waves in the baseline subtraction. Aryan *et al*. (2016) proposed to use 3D laser vibrometry to measure displacement/velocity fields near actuator. The measured displacement/velocity fields are then used in finite element (FE) simulations to reconstruct the reference signals for baseline subtraction. To avoid the dependence of reference signals, research has also focused on developing reference-free damage detection methods such as time-reversal technique (Park *et al*. 2007; Gangadharan *et al*. 2009).

Recent studies have focused on the use of nonlinear feature of guided waves, e.g. higher harmonic generation, to minimise or avoid the dependence of the damage detection techniques on the reference signals. Different damage detection techniques have been

developed using the phenomenon of higher harmonic generation. Soleimanpour *et al*. (2017) investigated the higher harmonic generation at delaminations in laminated composite beams. Shen and Cesnik (2017) studied the higher harmonic generation at fatigue cracks using the local interaction simulation approach. Yelve *et al*. (2017) employed the higher harmonic generation to detect the delamination in composite laminates. He and Ng (2017) proposed a time-domain spectral finite element method to investigate the higher harmonic generation at breathing crack in beams. Yang *et al*. (2018) studied the effect of fatigue crack opening and incident wave angle on the second harmonic generation of Lamb waves. The study was extended to investigate the second harmonic generation of guided wave at crack-induced debonding in metallic plates strengthened by fibre-reinforced polymer.

Scattering analysis of damage in composite laminates

The focus of this study is on scattering analysis of Lamb waves at damage in composite laminates, which provides the fundamental understanding of using Lamb waves in damage detection for composite laminates. In the literature, different studied have been carried out and focused on this aspect. Ramadas *et al*. (2009) investigated the mode conversion effect. They studied incident fundamental anti-symmetric mode (A_0) Lamb wave interacts at the entrance of a symmetric delamination, by which the fundamental symmetric mode (S_0) Lamb wave is generated and travels within each of the sub-laminate at the delamination. Ramadas *et al*. (2010) then extended their study to asymmetrically located delamination in the composite laminates. It was observed that, in the case of symmetrically located delaminations, the newly generated A_0-S_0 wave is confined to the sub-laminates. In the case of asymmetrically located delaminations, it is able to observe the mode converted S_0 wave in both the reflected side and the transmitted side of the composite laminate. This phenomenon

was studied numerically on a 2D model and the results were compared with experimental results.

Veidt and Ng (2011) proposed a 3D FE model to predict the A_0 Lamb wave scattering at the through hole in the composite laminates. Both numerical simulations and experimental measurements were used to investigate the characteristics of A_0 Lamb wave scattering at the through hole. Leckey *et al*. (2014) proposed a 3D elastodynamic finite integration technique to investigate the guided wave propagation and scattering at the delamination in the composite laminate. Experiments using laser vibrometer were also carried out in their study. Murat *et al*. (2016) investigated the A_0 Lamb wave scattering at the delamination in the composite laminates. Both 3D FE simulations and experiments were carried in the study. Their study mainly focuses on the mixed-mode defects and impact damage. Gupta and Rajagopal (2018) employed the FE simulation and experimental measurement to investigate the S_0 Lamb wave interaction at delaminations in the composite laminates. However, there are limited studies focused on mode conversion effect of Lamb wave scattering at the delamination in the composite laminates. This study employs the 3D FE simulations to investigate the A_0 Lamb wave scattering and mode conversion at the delaminations in composite laminates. The effect of the delamination size and through-thickness location of the delamination are investigated in this study.

The paper is organized as follows. The 3D explicit FE model is first presented in the next section. It provides a detailed description of the FE modelling. The experimental setup and the results obtained are described and compared with the results calculated by the 3D FE model. After that a series of numerical case studies are presented, in which different sizes of delaminations and through-thickness locations are considered. Finally, a conclusion is provided in the last section to summarize the work done in this paper.

Three-dimensional Explicit Finite Element Simulation

A 3D FE model is developed to simulate the Lamb wave propagation, A_0 scattering and mode conversion from A_0 to S_0 wave at the delaminations in a quasi-isotropic (QI) composite laminate. A commercial software, ABAQUS, was used to generate the geometry of the QI composite laminate and perform the meshing of the FE model. The in-plane dimension of the QI composite laminate is 200×250mm^2. It is assumed that the QI composite laminate is made by eight Epoxide EHM-32 unidirectional carbon/epoxy prepreg tapes with stacking sequence of $[-45/45/0/90]_S$ (Ng *et al*. 2017a; Ng *et al*. 2017b). The elastic properties of the Epoxide EHM-32 are shown in Table 1, and the density and fibre volume fraction is 1300kg/m^3 and 0.52, respectively. The thickness of each lamina is 0.2mm, and hence, the total thickness of the QI composite laminate is 1.6mm.

[Table 1. Elastic properties of Epoxide EHM-32 prepare lamina]

Absorbing layers by increasing damping (ALID) (Drozdz *et al*. 2006; Rajagopal et al. 2012; Mohseni & Ng 2019) are modelled at three edges of the QI composite laminate as shown in Figure 1. A PZT is modelled on the fourth. This edge will therefore not contain a damping layer. ALID contains different layers of elements with gradually varying damping to absorb the wave passing through these layers. The purpose of the ALID is to avoid the wave reflected from the boundaries of the QI composite laminate. Therefore, the A_0 scattered wave and A_0-S_0 mode converted wave can be extracted while the size of the FE model can be minimised to reduce the computational cost. The width of the ALID is 50mm, which contains 25 layers and the width of each layer is 2mm. In this study, the mass-proportional damping is used to model the ALID. A high rate of varying damping value for the ALID would create stiff material layers and generate reflected wave. A low rate of damping value, on the other

hand, would lead to incomplete absorption of the wave. In this study, the values of the mass-proportional damping (α) across the ALID are calculated by (Rajagopal et al. 2012; Mohseni & Ng 2019)

$$\alpha(x) = \alpha_{max} X(x)^P \quad (1)$$

where x is the location from the boundary between the QI composite lamination and ALID. P=3 and α_{max}=3×10^6 are used in this study. Taking into account the ALID, the total in-dimension of the FE model is 300×300mm^2.

[Figure 1. Schematic diagram of the 3D FE model]

3D 4-node fully integration shell elements (S4) are used in the FE model. Each node of the shell elements has three translation degrees-of-freedom (DoFs) and three rotation DoFs. Two layers of shell elements are connected by tie constraint to model the QI composite laminate. The delamination is created by removing the tie constraint over the delamination area (Monseni & Ng 2018). The thickness and number of laminae of the two layers of shell elements depend on the through-thickness location of the delamination. The size of shell elements used in the 3D FE model is around 0.5×0.5mm^2.

In this study, the A_0 Lamb wave is assumed to be excited by a 10mm diameter and 2mm thick half circular piezoceramic transducer. Based on the polar coordinator shown in Figure 1, the piezoceramic transducer is located at r=125mm and θ=180°. The piezoceramic transducer is not modelled in the FE model, but the excitation is modelled by applying the out-of-plane nodal displacement to the nodal points covered by the assumed piezoceramic transducer. The excitation signal is 120kHz narrow-band five-cycle sinusoidal tone burst pulse modulated by a Hanning window. For calculating the A_0 scattered wave and A_0-S_0 mode converted wave, the out-of-plane and in-plane displacements were recorded at 36 nodal

points, one for every 10^o at a constant distance from the centre of the damage. All explicit dynamic simulations were solved by ABAQUS/Explicit. The time step was automatically controlled by ABAQUS/Explicit.

Experimental Setup

An eight-ply QI composite laminate specimen was manufactured and the dimension of the specimen is 800×800×1.6mm^3. The QI composite laminate was made by Eporite EHM-32 unidirectional carbon/epoxy prepreg tapes and the stacking sequence is $[-45/45/0/90]_S$. The elastic properties are the same as in Table 1, and the fibre volume faction and stacking sequence are identical to the FE model described in the Section "Three-dimensional Explicit Finite Element Simulation".

A 10mm diameter and 2mm thick circular piezoceramic transducer was used to generate the A_0 incident Lamb wave. A 3mm thick brass mass with the same diameter was attached on the top of the piezoceramic transducer as a backing mass to increase the excitability of the A_0 Lamb wave. The piezoceramic transducer was bonded to the surface of the QI composite laminate using conductive epoxy and the centre of the transducer is located at r=125mm and θ=180°, which is identical to the FE model. Figure 2 shows a schematic diagram of the experimental setup. The excitation signal is a 10V peak-to-peak narrow-band five-cycle sinusoidal tone burst pulse modulated by a Hanning window. This excitation signal generated by a computer controlled arbitrary waveform generator is amplified by a power amplifier by a factor of 10-50 before it was sent to the piezoceramic transducer. A Polytec laser vibrometer was used to measure the Lamb wave signals. The measured data was then used to calculate the mode tuning curve, group velocity dispersion curve, directivity pattern of the incident wave, and the attenuation of the incident Lamb wave against the wave propagation distance.

[Figure 2. Schematic diagram of experiment setup]

The excitation frequency was chosen to be 120kHz, which was decided based on the results obtained from the mode tuning analysis. The incident wave was generated by the piezoceramic transducer at frequency from 60kHz to 160kHz in steps of 10kHz, and the generated Lamb waves were measured at a fixed location away from the piezoceramic transducer using the laser vibrometer. At each excitation frequency, the amplitudes of S_0 and A_0 were recorded. Figure 3 shows the results of the mode tuning analysis. At 120kHz, the generated incident wave has a relatively high A_0 amplitude to S_0 amplitude ratio, and the measured signal has the minimum level of noise. Therefore, 120kHz was chosen in this study. The wavelength of A_0 Lamb wave at 120kHz is around 8.64mm.

[Figure 3: Mode tuning curve of a 2mm thick PZT with a 3 mm thick brass backing mass]

Lamb wave propagation properties

A circular measurement configuration with 100mm radius and centre located at the piezoceramic transducer was used to measure the incident A_0 Lamb wave amplitudes at different directions at 120kHz. There are 36 measurement points in the circular measurement configuration and they are 10° away from each other. After the displacements were measured at these locations, the absolute amplitudes of the incident A_0 Lamb wave were extracted and the amplitude at each direction is normalised by the mean of the maximum absolute amplitudes of all directions. Figure 4 shows the experimentally measured and numerical results. The figure shows that the numerical results have reasonable agreement with the experimentally measured results.

[Figure 4: Normalized polar directivity pattern of the maximum absolute amplitude of the incident A_o wave at 120kHz in a $[-45/45/0/90]_S$ composite laminate]

The attenuation property of the incident A_0 Lamb wave at 120kHz and in θ=0° direction was experimentally measured and computationally simulated. The out-of-plane displacements were obtained from 20mm to 100mm away from the piezoceramic transducer and the step increment is 10mm. Figure 5 shows the experimentally measured and computationally simulated amplitude of the incident A_0 Lamb wave. The amplitude is normalized by the amplitude measured at 20mm away from the piezoceramic transducer. The results show that the attenuation property of the FE simulated A_0 Lamb wave has good agreement with the experimentally measured data.

[Figure 5: Normalized out-of-plane displacement amplitude as a function of wave propagation distance at $\theta=0°$ and 120kHz]

Figure 6 shows that group velocity dispersion curve in θ=0° direction. Both experimentally measured and computationally simulated group velocities are shown in the figure. The group velocity curve were obtained by sweeping the excitation frequency from 60kHz to 160kHz in steps of 20kHz. The group velocities calculated by DISPERSE software are also shown in Figure 6. The results show that the computationally simulated group velocities have good agreement with the theoretical and experimental results for both S_0 and A_0 Lamb wave. The results show that the 3D FE model is able to provide correct prediction for the S_0 and A_0 Lamb wave propagation.

[Figure 6. Group velocity dispersion curve at θ=0°]

Numerical case studies

The 3D FE model described in the Section "Three-dimensional Explicit Finite Element Model" is used to study the A_0 scattered and A_0-S_0 mode converted Lamb wave at the delaminations in a series of numerical case studies. The in-plane and out-of-plane nodal displacements at r=80mm and 0°≤θ≤360° (as shown in Figure 1) with 10° step increment are calculated using the 3D FE model. In this study, the baseline subtraction approach is used to extract the A_0 scattered and A_0-S_0 mode converted Lamb wave. The baseline subtraction approach requires two simulations, intact model and model with the delamination, and the FE meshes of these two models are identical. The A_0 scattered and A_0-S_0 mode converted Lamb wave at the delamination can be calculated by

$$u_{r,\theta}^{(S)}(t) = u_{r,\theta}^{(D)}(t) - u_{r,\theta}^{(U)}(t) \tag{2}$$

$$v_{r,\theta}^{(S)}(t) = v_{r,\theta}^{(D)}(t) - v_{r,\theta}^{(U)}(t) \tag{3}$$

where the u and v are the in-plane and out-of-plane nodal displacement respectively. The superscripts (S), (D) and (U) means the scattered signal, and signal obtained from model with and without the delamination, respectively. $v_{r,\theta}^{(S)}$ is the A_0 scattered Lamb wave and $u_{r,\theta}^{(S)}$ is the A_0-S_0 mode converted Lamb wave. In this study, the amplitude of the A_0 scattered Lamb wave and A_0-S_0 mode converted Lamb wave are normalized as

$$\bar{u}_{r,\theta}^{(S)} = \frac{\left|u_{r,\theta}^{(S)}\right|}{max\left(\left|v_{0,\theta}^{(U)}\right|\right)} \tag{4}$$

$$\bar{v}_{r,\theta}^{(S)} = \frac{\left|v_{r,\theta}^{(S)}\right|}{max\left(\left|v_{0,\theta}^{(U)}\right|\right)} \tag{5}$$

where $v_{0,\theta}^{(U)}$ is the out-of-plane displacement at the delamination centre location obtained from the model without the delamination.

A_0 scattered Lamb wave

This section investigates the A_0 Lamb wave scattering and A_0-S_0 mode conversion at different sizes of delaminations. The delaminations are all located between third and fourth lamina. The scattering directivity pattern (SDP) (Veidt and Ng 2011) of the A_0 scattered and A_0-S_0 mode converted Lamb wave are used to present the results. Figure 7 shows the SDP of the A_0 scattered wave at the delaminations. Figures 7a-d show the SDPs for the 7.5mm, 12.5mm, 17.5mm and 20mm diameter delaminations, respectively. The results show that the amplitude of A_0 scattered wave depends on the stacking sequence of the composite laminate. In this study, the fibre orientations at the outer laminae are -45° and 45° and the scattering wave energy focuses around these two directions. This phenomenon is consistent with the finding in Veidt and Ng (2011). For larger size of the delamination, the energy of the A_0 scattered wave tends to be mainly focused in the forward directions.

[Figure 7. SDP of A_0 scattered wave for a) 7.5mm, b) 12.5mm, c) 17.5mm and d) 20mm diameter delamination located between 3rd and 4th lamina]

A_0-S_0 mode converted Lamb wave

In addition to the A_0 scattered Lamb wave, the A_0-S_0 mode converted Lamb wave at these delaminations is also calculated and the results are shown in Figure 8. The SDP of the A_0-S_0 mode converted Lamb wave and the amplitudes are normalized using Equation (4). As shown in Figure 8, the amplitude of the A_0-S_0 mode converted wave is smaller than the A_0 scattered

Lamb wave. This indicates when the A_0 Lamb wave interacts with the delamination, it produces A_0-S_0 mode converted Lamb wave, but the energy is small. The SDP shown in Figure 8 indicates that the A_0-S_0 mode converted Lamb wave is also influenced by the stacking sequence of the composite laminates. Similar to the A_0 scattered wave, the energy of the A_0-S_0 mode converted Lamb wave mainly focuses around fibre orientation of the outer laminae, i.e. at -45° and 45°. For larger size of delamination, the A_0-S_0 mode converted Lamb wave has larger amplitude.

[Figure 8. SDP of A_0-S_0 mode converted wave for a) 7.5mm, b) 12.5mm, c) 17.5mm and d) 20mm diameter delamination located between 3rd and 4th lamina]

Effect of delamination size

A further investigation was carried to study the characteristics of the A_0 scattered and A_0-S_0 mode converted Lamb wave. Different sizes of delamination are considered in this study. Without loss of generality, the study is in terms of delamination diameter to A_0 incident wave wavelength ratio (R_{DW}). The range of the R_{DW} considered is from 0.58 to 2.31, which covers seven sizes of delaminations. Figures 9a and 9b show the forward (θ=0°, 20°, 40°, 320° and 340°) and backward (θ=140°, 160°, 180°, 200° and 220°) A_0 scattered Lamb wave. In general, the amplitudes of the A_0 scattered wave in forward direction are larger than backward direction, especially when the R_{DW} become larger. In the forward direction, for the A_0 scattered wave, the amplitudes increase linearly with R_{DW}. There is a small variation at some specific directions, i.e. θ=180° and 200°, but trends of the amplitudes in the backward directions are in general increase with R_{DW}.

[Figure 9. Normalized amplitude for the a) forward and b) backward A_0 scattered wave]

Figures 10a and 10b show the corresponding forward and backward A_0-S_0 mode converted Lamb wave for different sizes of delaminations. The amplitude of A_0-S_0 mode converted Lamb wave is always smaller than the A_0 scattered Lamb wave. In general, the amplitude of the A_0-AS_0 mode converted Lamb wave has an increasing trend with variation.

[Figure 10. Normalized amplitude for the a) forward and b) backward A_0-S_0 mode converted Lamb wave]

Effect of through-thickness location of delamination

In this section, the effect of through-thickness location of delamination is investigated. A fixed size of delamination (20mm diameter) is simulated at different through-thickness locations. The SDP of the A_0 scattered and A_0-S_0 mode converted Lamb wave are shown in Figures 11 and 12, respectively. Figures 11a, 11b and 11c show the SDP of A_0 scattered wave at delamination located between, first and second, second and third, and third and fourth layers, respectively. Since the 20mm diameter delamination is considered as a large damage, the energy of the A_0 scattered wave mainly focuses in the forward direction. Figures 12a, 12b and 12c show the corresponding SDP of the A_0-S_0 mode converted Lamb wave. The energy of the mode converted wave also depends on the fibre orientation of the outer laminae.

[Figure 11. SDP of A_0 scattered wave for a 20mm diameter delamination located between a) 1^{st} and 2^{nd} , b) 2^{nd} and 3^{rd}, and c) 3^{rd} and 4^{th} lamina]

[Figure 12. SDP of A_0-S_0 mode converted wave for a 20mm diameter delamination located between a) 1^{st} and 2^{nd} , b) 2^{nd} and 3^{rd}, and c) 3^{rd} and 4^{th} lamina]

Conclusions

This paper has investigated the scattering and mode conversion of Lamb wave at the delaminations in the $[-45/45/0/90]_S$ QI composite laminate. The A_0 Lamb wave has been used as incident wave and the A_0 scattered and A_0-S_0 mode converted Lamb wave have been studied in details. A 3D FE model has been proposed to predict the wave propagation, scattering and mode conversion at the delamination. An experimental study has been carried out and the results have shown that the 3D FE model is able to provide a reasonable prediction of A_0 and S_0 Lamb wave propagation. A series of numerical case studies have been carried out to investigate the A_0 scattered and A_0-S_0 mode converted Lamb wave characteristics at the delamination using the 3D FE model. From the results of the SDPs, it has been shown that both A_0 scattered and A_0-S_0 mode converted Lamb wave are influenced by the fibre orientation of the outer laminae. In general, the amplitude A_0 scattered and A_0-S_0 mode converted Lamb wave have an increasing trend with the delamination size. Finally, the effect of the through-thickness location of the delamination on the A_0 scattered and A_0-S_0 mode converted Lamb wave has also been demonstrated using the SDP. Overall, the findings of this study can provide improved physical insight into the scattering and mode conversion of Lamb wave at delamination. The results can help further develop the delamination detection techniques in the composite laminate.

References

Aryan, P. Kotousov, A., Ng, C.T., Cazzolato, B.S. 2017. “A baseline-free and non-contact method for detection and imaging of structural damage using 3D laser vibrometry.” *Structural Control and health Monitoring* 24(4): e1894.

Aryan, P., Kotousov, A., Ng, C.T., Wildy, S. 2016. “Reconstruction of baseline time-trace under changing environmental and operational conditions.” *Smart Materials and Structures* 25: 035018.

Avdelidis, N.P., Hawtin, B.C. and Almond, D.P. 2003. “Transient thermography in the assessment of defects of aircraft composites.” *NDT&E International* 36(6): 433-439.

Cegla, F.B., Rohde, A., and Veidt, M. 2008. “Analytical prediction and experimental measurement for mode conversion and scattering of plate waves at non-symmetric circular blind holes in isotropic plates.” *Wave Motion* 45: 162-177.

Croxford, A.J., Moll, J., Wilcox, P.D., Michaels, J.E., 2010. “Efficient temperature compensation strategies for guided wave structural health monitoring.” *Ultrasonics* 50(4-5): 517-528.

Diamanti, K. Hodgkinson, J.M. and Soutis, C. 2004. “Detection of low-velocity impact damage in composite plates using Lamb wave.” *Structural Health Monitoring* 3(1): 33-41.

Diligent, O., Grahn, T. and Bostrom, A. 2002. “The low-frequency reflection and scattering of the S_0 Lamb mode from a circular through-thickness hole in a plate: finite element, analytical and experimental studies.” *Journal of the Acoustical Society of America* 112: 2589-2601.

Drozdz, M., Moreau, L., Castaings, M., Lowe, M.J.S. and Cawley, P. 2006. “Efficient numerical modelling of absorbing regions for boundaries of guided wave problems.” *AIP Conference Proceedings* 820(1): 126-133:

Flores-Lopez, M.A. and Gregory, R.D. 2006. “Scattering of Rayleigh-Lamb waves by a surface breaking crack in an elastic plate.” *Journal of Acoustical Society of America* 119: 2041-2049.

Fromme, P. and Sayir, M.B. 2002. “Measurement of the scattering of a Lamb wave by a through hole in plate,” *Journal of Acoustical Society of America* 111: 1165–1170.

Gangadharan, R., Murthy, C.R.L., Gopalakrishnan, S., Bhat, M.R. 2009. “Time reversal technique for health monitoring of metallic structure using Lamb waves.” *Ultrasonics* 49(8): 696-705.

Grahn, T. 2003. “Lamb wave scattering from a circular partly through-thickness hole in a plate.” *Wave Motion* 37(1): 63-80.

Gupta, S. and Rajagopal, P. 2018. “Effect of ply orientation and through-thickness position of delamination on the reflection of fundamental symmetric S_0 Lamb mode in GFRP composite plate structures.” *Ultrasonics* 90: 109-119.

He, S. and Ng, C.T. 2016. “A probabilistic approach for quantitative identification of multiple delaminations in laminated composite beams using guided waves.” *Engineering Structures* 127: 602-614.

He, S. and Ng, C.T. 2017. “Guided wave-based identification of multiple cracks in beams using a Bayesian approach.” *Mechanical Systems and Signal Processing* 84: 324-345.

He, S. and Ng, C.T. 2017. “Modelling and analysis of nonlinear guided waves interaction at a breathing crack using time-domain spectral finite element method.” *Smart Materials and Structures* 26: 085002.

Hollaway, L.C. 2010. “A review of the present and future utilisation of FRP composites in the civil infrastructure with reference to their important in-service properties.” *Construction and Building Materials* 24(12): 2419-2445.

Ibrahim, M.E. 2014. “Nondestructive evaluation of thick-section composites and sandwich structures; a review.” *Composites Part A: Applied Science and Manufacturing* 64: 36-48.

Imielinska, K., Castaings, M., Wojtyra, R. Haras, J., Le Clezio, E. and Hosten, B. 2004. “Air-coupled ultrasonic C-scan technique in impact response testing of carbon fibre and hybrid: glass, carbon and Kevlar/epoxy composite laminates.” *Journal of Materials Processing Technology*.” 157-158: 513-522.

Kazys, R. and Svilainis, L. 1997. “Ultrasonic detection and characterization of delaminations in thin composite plates using signal processing techniques.” *Ultrasonics* 35(5): 367-383.

Kessler, S.S, Spearing, S.M. and Soutis, C. 2002. “Damage detection in composite materials using Lamb wave methods.” *Smart Materials and Structures* 11: 269-278.

Leckey, C.A.C., Rogge, M.D. and Parker, F.R. 2014. “Guided waves in anisotropic and quasi-isotropic aerospace composites: three-dimensional simulation and experiment.” *Ultrasonics* 54(1): 385-394.

Liu, Z., Li, P., Srikanth, N. 2019. “Effect of delamination on the flexural response of $[+45/-45/0]_{2s}$ carbon fibre reinforced polymer laminates.” *Composite Structures* 209: 93-102.

Lu, G., Li, Y., Wang, T., Xiao, H., Huo, L., Song, G. 2017. “A multi-delay-and-sum imaging algorithm for damage detection using piezoceramic transducer.” *Journal of Intelligent Material Systems and Structures* 28(9): 1150-1159.

Mizukami, K., Mizutani, Y., Todoroki, A. and Suzuki, Y. 2015. “Detection of delamination in thermoplastic CFRP welded zones using induction heating assisted eddy current testing.” *NDT&E International* 74: 106-111.

Mohseni, H. and Ng, C.T. 2018. “Higher harmonic generation of Rayleigh wave at debondings in FRP-retrofitted concrete structures.” *Smart Materials and Structures* 27: 105038.

Mohseni, H. and Ng, C.T. 2019. “Rayleigh wave propagation and scattering characteristics at debondings in fibre-reinforced polymer-retrofitted concrete structures.” *Structural Health Monitoring* 18(1): 303-317.

Mook, G., Lange, R. and Koeser, O. 2001. “Non-destructive characterisation of carbon-fibre-reinforced plastics by means of eddy-current.” *Composite Science and Technology* 61(6): 865-873.

Moreau L., Velichko, A. and Wilcox, P.D. 2012. “Accurate finite element modelling of guided wave scattering from irregular defects.” *NDT&E International* 45, 46–54.

Murat, B.I.S., Khalili, P. and Fromme, P. 2016. “Scattering of guided waves at delaminations in composite plates.” *Journal of Acoustical Society of America* 139(6): 3044-3052.

Ng, C.T. 2015a. “A two-stage approach for quantitative damage imaging in metallic plates using Lamb waves.” *Earthquakes and Structures* 8(4): 821-841.

Ng, C.T. 2015b. “On accuracy of analytical modelling of Lamb wave scattering at delaminations in multi-layered isotropic plates.” *International Journal of Structural Stability and Dynamics* 15(8): 1540010.

Ng, C.T., Pudipeddi, G.T. and Kotousov, A. 2017a. “3D finite element prediction of scattering and mode conversion of Lamb waves at delaminations in composite laminates.” *In Proc. 8th Int. Conf. on Structural Health Monitoring of Intelligent Infrastructure (SHMII-8),* Brisbane, Australia.

Ng, C.T., Pudipeddi, G.T. and Kotousov, A. 2017b. “Numerical simulation and experimental verification of Lamb wave scattering and model conversion at delaminations in composite laminates.” *In Proc. 9th Australasian Congress on Applied Mechanics (ACAM9)*: 533-539, Sydney, Australia.

Pan, J., Zhang, Z., Wu, J., Ramakrishnan, K.R. and Singh, H.K. 2018. “A novel method of vibration modes selection for improving accuracy of frequency-based damage detection.” *Composite Part B: Engineering* 159: 437-446.

Park, H.W., Sohn, H., Law, K.H. and Farrar, C.R. 2007. “Time reversal active sensing for health monitoring of a composite plate.” *Journal of Sound and vibration* 302(1-2): 50-66.

Pieczonka, L., Ambrozinski, L., Staszewski, W.J., Barnoncel, D., Peres, P. (2017). "Damage detection in composite panels based on mode-converted Lmab waves sensed using 3D laser scanning vibrometer." *Optics and Lasers in Engineering* 99: 80-87.

Rajagopal, P., Drozdz, M., Skelton, E.A., Lowe, M.J.S. and Craster, R.V. 2012. "On the use of absorbing layers to simulate the propagation of elastic waves in unbounded isotropic media using commercial available finite element packages." *NDT&E International* 51: 30-40.

Ramadas, C., Balasubramaniam, K., Joshi, M. and Krishnamurthy, CV. (2009), "Interaction of primary anti-symmetric Lamb mode with symmetric delaminations: numerical and experimental studies." *Smart Material and Structures* 18(8): 085011.

Ramadas, C., Balasubramaniam, K., Joshi. M. and Krishnamurthy. C.V. (2010), "Interaction of guided Lamb waves with an asymmetrically located delamination in a laminated composite plate." *Smart Material and Structures* 19(6): 065009.

Ratassepp, M., Lowe, M.J.S., Cawley, P. and Klauson, A. 2008. "Scattering of the fundamental shear horizontal mode in a plate when incident at a through crack aligned in the propagation direction of the mode." *Journal of Acoustical Society of America* 124: 2873-2882.

Shen, Y. and Cesnik, C.E. 2017. "Modelling of nonlinear interactions between guided waves and fatigue cracks using local interaction simulation approach." *Ultrasonics* 74: 106-123.

Sherafat, M.H., Quaegebeur, N., Hubert, P., Lessard, L. and Masson, P. 2018. "Experimental model of impact damage for guided wave-based inspection of composites." *ASME Journal of Nondestructive Evaluation* 1(4): 040801.

Singh, R.K., Ramadas, C., Shetty, P.B., Satyanarayana, K.G. 2017. "Identification of delamination interface in composite laminates using scattering characteristics of Lamb wave: numerical and experimental studies." *Smart Materials and Structures* 26(4): 045017.

Sinha, A., Sastry, O.S. and Gupta, R. 2015. "Detection and characterisation of delamination in PV modules by active infrared thermography." *Nondestructive Testing and Evaluation* 31(1): 1-16.

Solemanpour, R. and Ng, C.T. 2017. "Locating delaminations in laminated composite beams using nonlinear guided wave." *Engineering Structures* 131: 207-219.

Solemanpour, R., Ng, C.T., Wang, C.H. 2017. “Higher harmonic generation of guided waves at delamination in laminated composite beams.” *Structural Health Monitoring* 16(45): 400-417.

Veidt, M. and Ng, C.T. 2011. “Influence of stacking sequence on scattering characteristics of the fundamental anti-symmetric Lamb wave at through hole in composite laminates.” *Journal of Acoustical Society of America* 129(3): 1280-1287.

Yang, B., Xuan, F.Z., Chen, S., Zhou, S., Gao, Y. and Xiao, B. 2017. “Damage localization and identification in WGF/epoxy composite laminates by using Lamb waves: experiment and simulation.” *Composite Structures* 165: 138-147.

Yang, Y., Ng, C.T., Kotousov, A. (2019). “Second harmonic generation of guided wave at crack-induced debonding in FRP-strengthened metallic plates.” *International Journal of Structural Stability and Dynamics* 19(10): 1940006.

Yang, Y., Ng, C.T., Kotousov, A. 2018. “Influence of crack opening and incident wave angle on second harmonic generation of Lamb waves.” *Smart Materials and Structures* 27: 055013.

Yang, Y., Ng, C.T., Kotousov, A., Sohn, H. and Lim, H.J. 2018. “Second harmonic generation at fatigue cracks by low-frequency Lamb waves: experimental and numerical studies.” *Mechanical Systems and Signal Processing* 99: 760-773.

Yelve, N.P., Mirtra, M. and Mujumdar, P.M. 2017. “Detection of delamination in composite laminates using Lamb wave based nonlinear method.” *Composite Structures* 159: 257-266.

Zhang, Z., Zhang, C., Shankar, K., Morozov, E.V., Singh, H.K. and Ray, T. 2017. “Sensitivity analysis of inverse algorithms for damage detection in composite.” *Composite Structures* 176: 844-859.

Zhang, Z., Zhang, C., Shankar, K., Morozov, E.V., Singh, H.K., Ray, T. “Sensitivity analysis of inverse algorithms for damage detection in composite.” *Composite Structures* 176: 844-859.

Figures

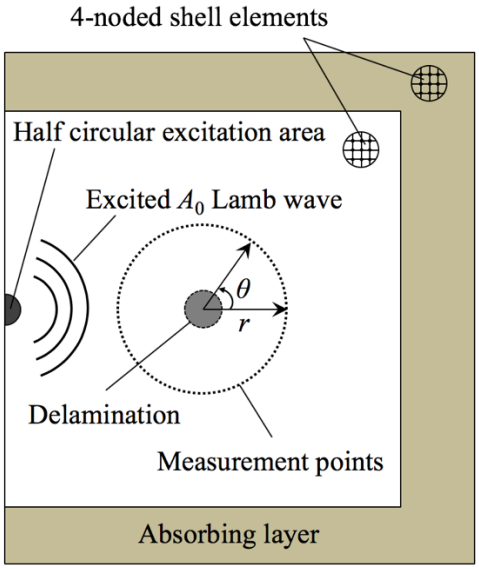

Figure 1. Schematic diagram of the 3D FE model

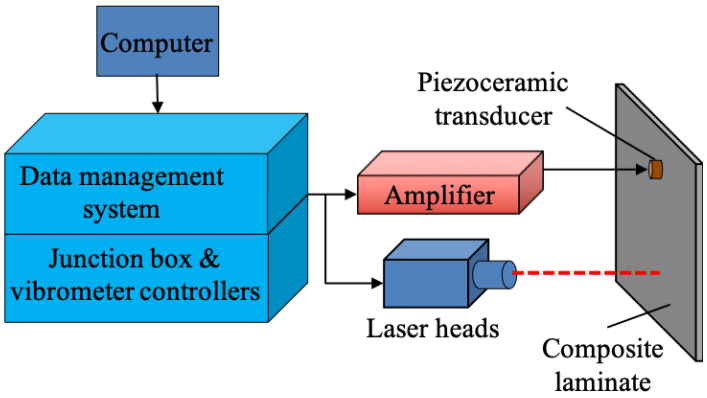

Figure 2. Schematic diagram of experiment setup

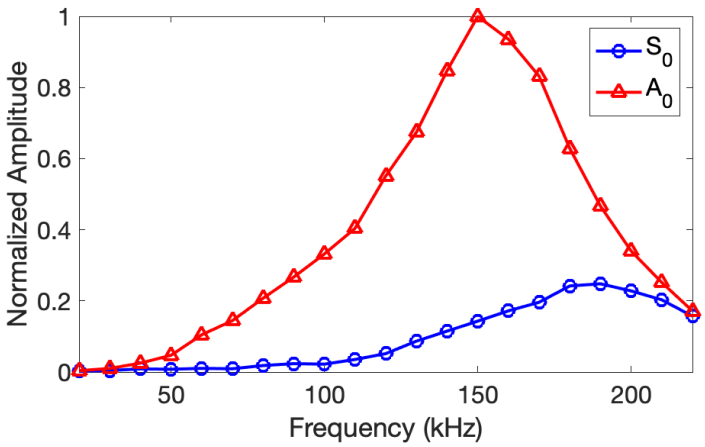

Figure 3: Mode tuning curve of a 2mm thick PZT with a 3mm thick brass backing mass

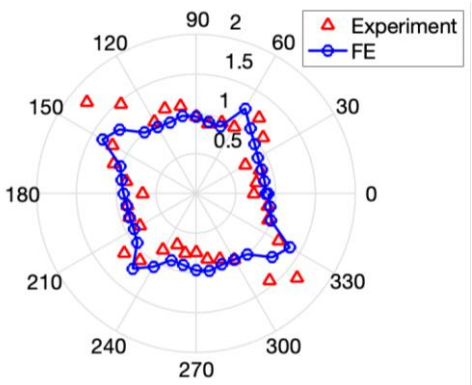

Figure 4: Normalized polar directivity pattern of the maximum absolute amplitude of the incident A_o wave at 120kHz in a $[-45/45/0/90]_S$ composite laminate

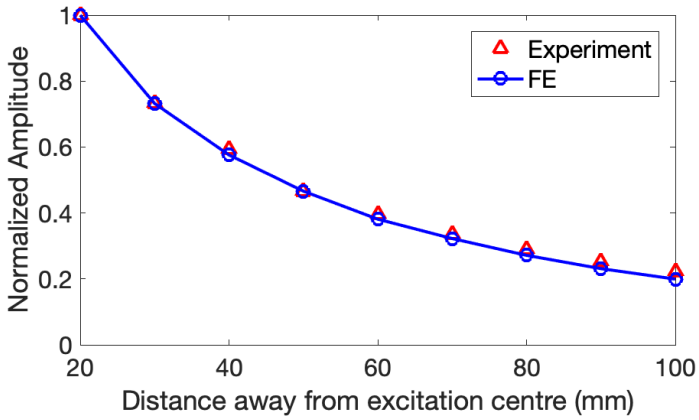

Figure 5: Normalized out-of-plane displacement amplitude as a function of wave propagation distance at θ=0° and 120kHz

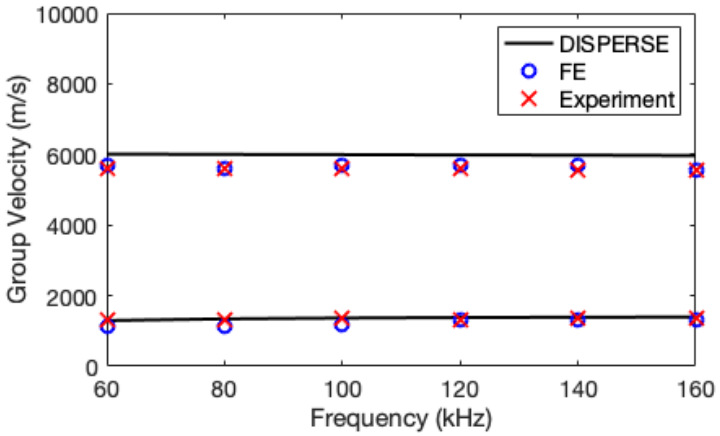

Figure 6. Group velocity dispersion curve at θ=0°

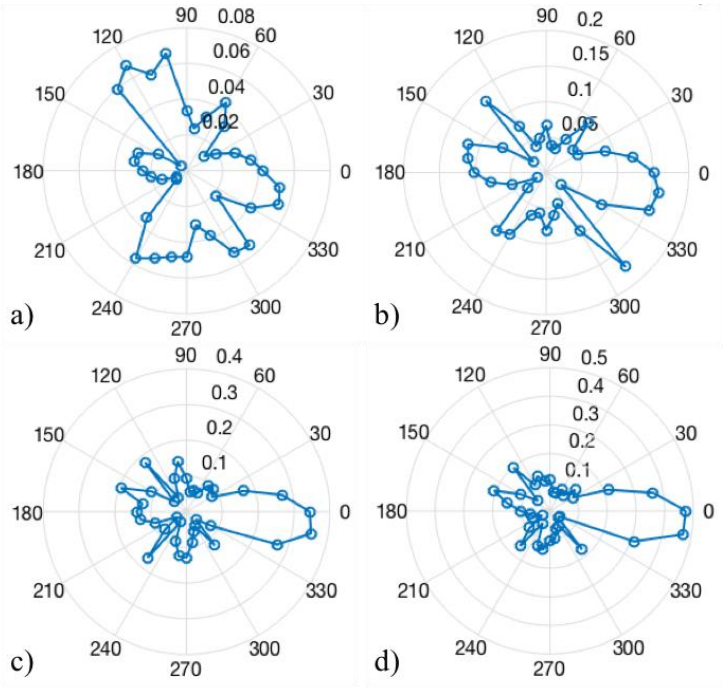

Figure 7. SDP of A_0 scattered wave for a) 7.5mm, b) 12.5mm, c) 17.5mm and d) 20mm diameter delamination located between 3rd and 4th lamina

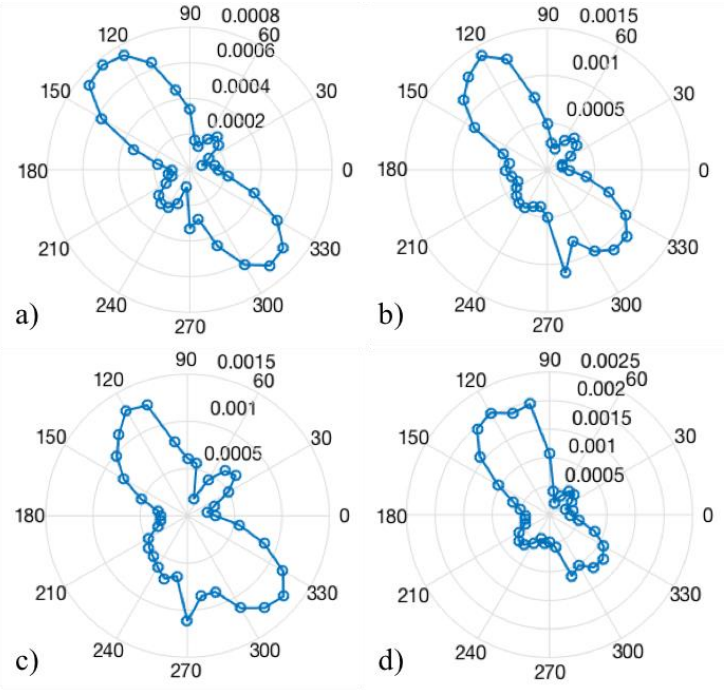

Figure 8. SDP of A_0-S_0 mode converted wave for a) 7.5mm, b) 12.5mm, c) 17.5mm and d) 20mm diameter delamination located between 3rd and 4th lamina

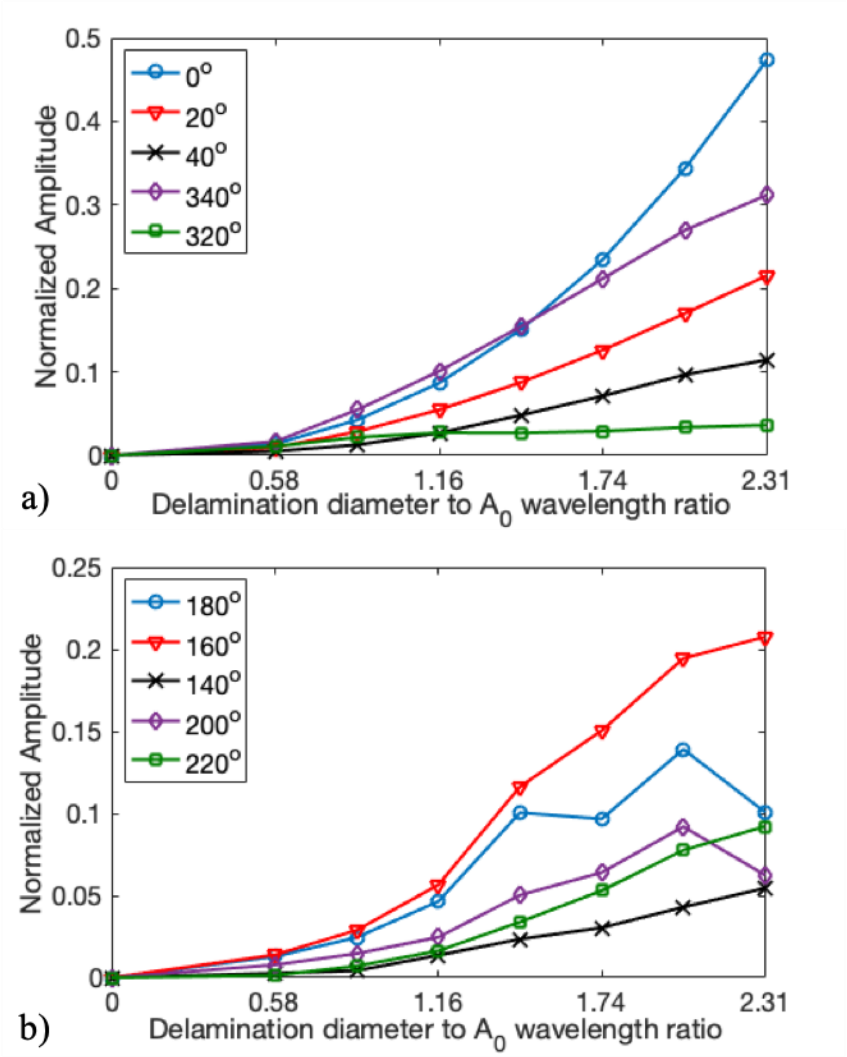

595
596 Figure 9. Normalized amplitude for the a) forward and b) backward A_0 scattered wave
597

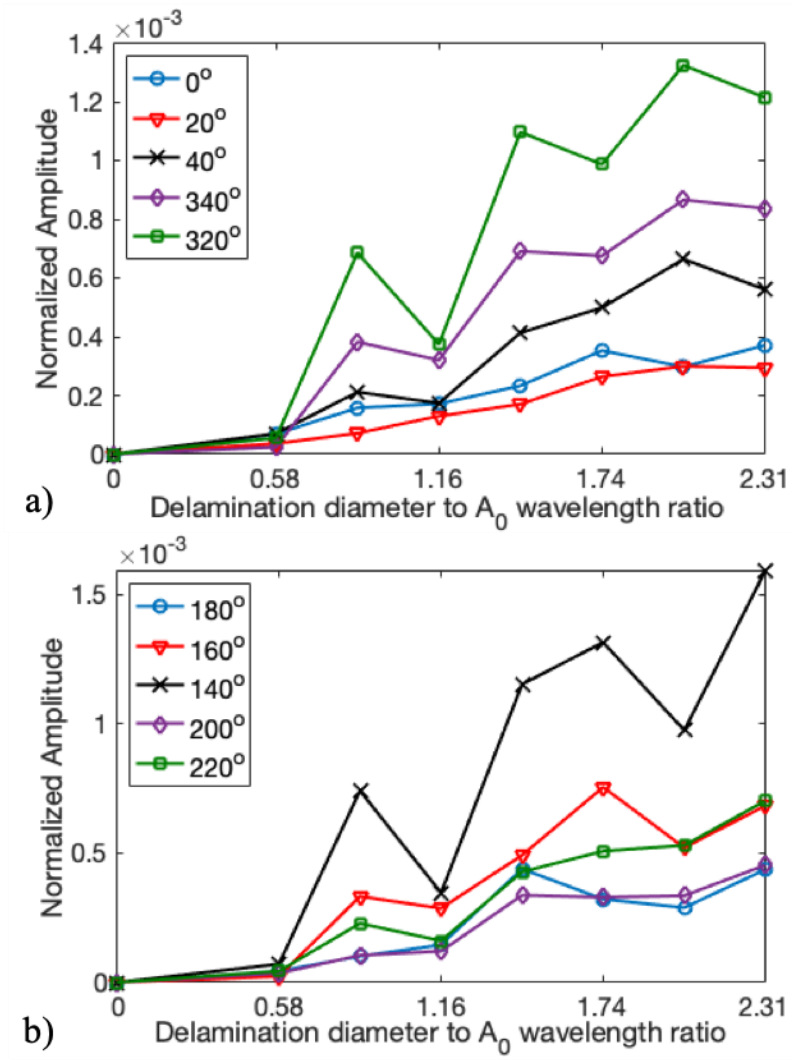

Figure 10. Normalized amplitude for the a) forward and b) backward A_0-S_0 mode converted Lamb wave

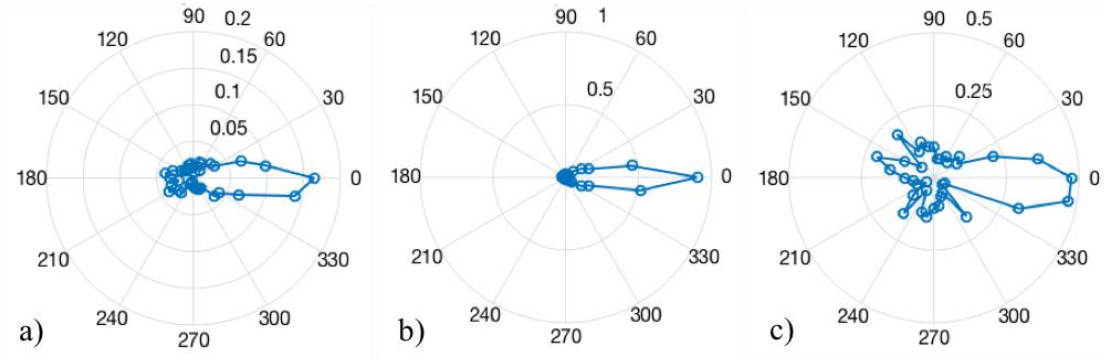

Figure 11. SDP of A_0 scattered wave for a 20mm diameter delamination located between a) 1st and 2nd , b) 2nd and 3rd, and c) 3rd and 4th lamina

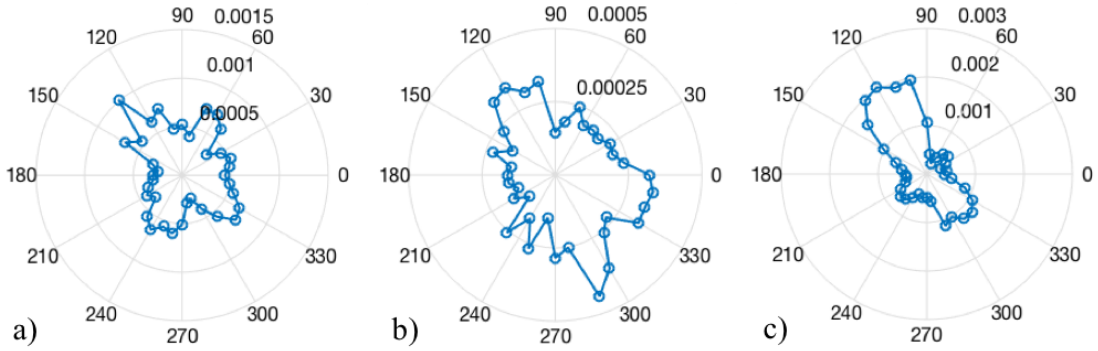

Figure 12. SDP of A_0-S_0 mode converted wave for a 20mm diameter delamination located between a) 1st and 2nd , b) 2nd and 3rd, and c) 3rd and 4th lamina

Tables

Table 1. Elastic properties of Epoxide EHM-32 prepare lamina

Young's moduli	E_{11}	111GPa
	E_{22}	7.16GPa
	E_{33}	7.16GPa
Shear moduli	G_{12}	3.52GPa
	G_{13}	3.52GPa
	G_{23}	2.2GPa
Poisson's ratios	ν_{12}	0.33
	ν_{13}	0.33
	ν_{23}	0.44